nature
Vol 439|5 January 2006|doi:10.1038/nature04276

LETTERS

Charon's radius and atmospheric constraints from observations of a stellar occultation

A. A. S. Gulbis[1], J. L. Elliot[1,2,3], M. J. Person[1], E. R. Adams[1], B. A. Babcock[4,6], M. Emilio[7], J. W. Gangestad[5,6], S. D. Kern[1], E. A. Kramer[1], D. J. Osip[8], J. M. Pasachoff[5], S. P. Souza[5] & T. Tuvikene[6,9]

The physical characteristics of Pluto and its moon, Charon, provide insight into the evolution of the outer Solar System. Although previous measurements have constrained the masses of these bodies[1,2], their radii and densities have remained uncertain. The observation of a stellar occultation by Charon in 1980 established a lower limit on its radius of 600 km (ref. 3) (later refined to 601.5 km; ref. 4) and suggested a possible atmosphere[4]. Subsequent, mutual event modelling yielded a range of 600–650 km (ref. 5), corresponding to a density of $1.56 \pm 0.22\,\mathrm{g\,cm^{-3}}$ (refs 2, 5). Here we report multiple-station observations of a stellar occultation by Charon. From these data, we find a mean radius of 606 ± 8 km, a bulk density of $1.72 \pm 0.15\,\mathrm{g\,cm^{-3}}$, and rock-mass fraction 0.63 ± 0.05. We do not detect a significant atmosphere and place 3σ upper limits on atmospheric number densities for candidate gases. These results seem to be consistent with collisional formation for the Pluto–Charon system in which the precursor objects may have been differentiated[6], and they leave open the possibility of atmospheric retention by the largest objects in the outer Solar System.

Observing light from a star as an object passes in front of it—a stellar occultation—produces data with the highest spatial resolution available from Earth-based observing methods. Such data are critical for determining accurate sizes and probing atmospheres of distant Solar System objects; however, observations can be difficult because of the required geographic and temporal precision. A stellar occultation by Charon has been observed only once before and resulted in a single chord[3].

An occultation by Charon of the star 'C313.2' (originally identified as a Pluto occultation candidate star 'P313.2'[7]; UCAC2 26257135, with R- and K-band magnitudes respectively $R = 14.8$ and $K = 12.2$) was predicted to occur on 11 July 2005 (UT) (http://occult.mit.edu/research/occultations/Charon/C313.2.html). We arranged to observe the event from four sites in South America using five telescopes. The telescopes were the 0.6-m at Laboratório Nacional de Astrofísica's Observatório Pico dos Dias, Itajubá, Brazil; the 0.84-m at Observatório Cerro Armazones, Antofagasta, Chile; the 2.5-m du Pont and 6.5-m Clay at Las Campanas Observatory, La Serena, Chile; and the 8-m Gemini South on Cerro Pachón, La Serena, Chile. Data were successfully obtained at all but Pico dos Dias, where the occultation was unobservable owing to clouds. The occultation occurred four days after new moon, and image quality ranged from excellent to poor at the successful observing stations (0.5–4 arcsec). The instruments employed for the observations, excluding Gemini South, were POETS (Portable Occultation, Eclipse, and Transit Systems). Each system consisted of a high-speed Andor Ixon camera, an instrument control computer, and a GPS receiver to trigger frames and establish accurate timing. Gemini South observations were performed using the Acquisition Camera. Observation details for each site are provided in Supplementary Information.

Charon's aspect at the time of the occultation is shown in Fig. 1, overlaid with the paths of each observed chord. The stations were spread approximately 580 km perpendicular to Charon's motion and spanned just under half of the shadow width, with stations on both sides of the centreline. Astrometric data were recorded at each successful site roughly an hour before and after the event, with twenty minutes of contiguous high-speed data encompassing the predicted midtimes. For reducing the data that spanned the occultation, a range of square apertures was selected, containing C313.2, Pluto and Charon. We used the astrometric frames, in which C313.2

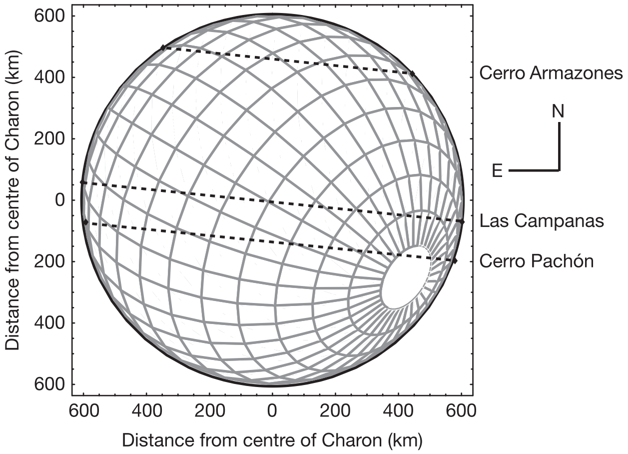

Figure 1 | Observed occultation chords. Overlaid on a diagram of Charon, dashed bold lines indicate the occultation chord paths as they appeared from each successful observing station. The coordinates (longitude, latitude) of each station are: Cerro Armazones (70° 11′ 46″ W, 24° 35′ 52″ S), Las Campanas du Pont (70° 42′ 13″ W, 29° 00′ 26″ S), Las Campanas Clay (70° 41′ 33″ W, 29° 00′ 51″ S) and Cerro Pachón (70° 43′ 24″ W, 30° 13′ 42″ S). Coordinates were obtained from POETS GPS surveys at all locations except Cerro Pachón, for which we reference the Astronomical Almanac[28]. The du Pont and Clay telescopes at Las Campanas are geographically close enough that their chords are indistinguishable in this plot. Charon's south pole (IAU coordinate convention) is visible in the lower right. The distance to Charon at the time of the occultation was 30.07 AU, and the geocentric shadow velocity was $20.93\,\mathrm{km\,s^{-1}}$. The geometric limb times during immersion and emersion for each of these chords were used to calculate Charon's radius.

---

[1]Department of Earth, Atmospheric, and Planetary Sciences, [2]Department of Physics, Massachusetts Institute of Technology, Cambridge, Massachusetts 02139-4307, USA. [3]Lowell Observatory, Flagstaff, Arizona 86001, USA. [4]Physics Department, [5]Astronomy Department, Williams College, Williamstown, Massachusetts 01267-2565, USA. [6]Instituto de Astronomía, Universidad Católica del Norte, Avda. Angamos 0610, Antofagasta, Chile. [7]Departamento de Geociências, Universidade Estadual de Ponta Grossa, Paraná, Brazil. [8]Las Campanas Observatory, Carnegie Observatories, Casilla 601, La Serena, Chile. [9]Vrije Universiteit Brussel, Brussels, Belgium.

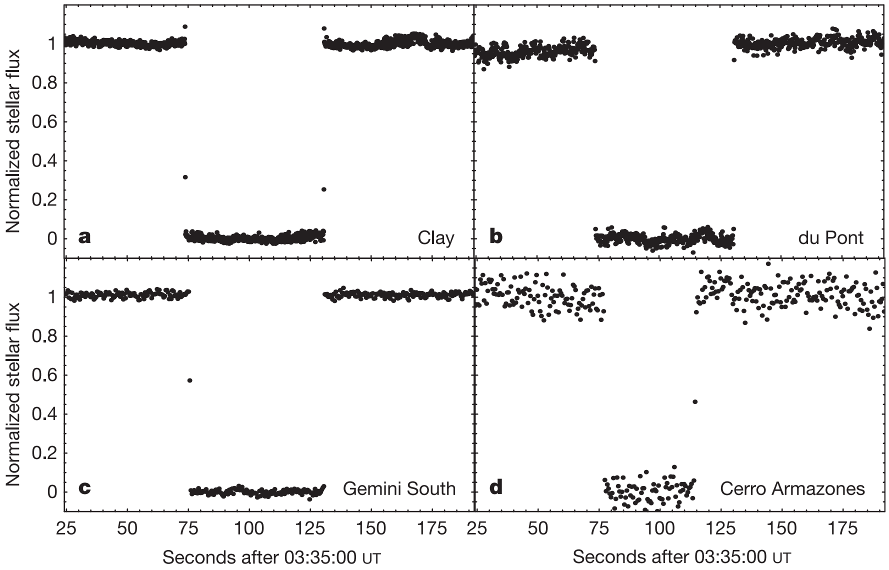

Figure 2 | Light curves showing the occultation of C313.2 by Charon. These plots display the normalized flux of the star observed at each of the four successful telescopes before, during and after the occultation. Telescopes and data rates for each of the plots are **a**, the Las Campanas 6.5-m Clay at 10 Hz, **b**, the Las Campanas 2.5-m du Pont at 5 Hz, **c**, the Cerro Pachón 8-m Gemini South at $\sim$2.24 Hz, and **d**, the Cerro Armazones 0.84-m telescope at 2 Hz. Excluding Gemini South, data were obtained using POETS (frame transfer time of 1.74 ms per exposure) and no filter. Gemini South employed the Acquisition Camera and the R_G0154 filter (610–750 nm), with an integration time of 0.3 s and 0.146 ± 0.001 s required for readout. The data points are plotted at the midpoint of each exposure, with respect to seconds after 03:35:00 UT. Geometric limb times from model fits to the light curves are **a**, immersion 73.744 ± 0.001 s, emersion 130.563 ± 0.002 s, **b**, immersion 73.792 ± 0.005 s, emersion 130.609 ± 0.004 s, **c**, immersion 75.50 ± 0.15 s, emersion 130.55 ± 0.15 s and **d**, immersion 76.99 ± 0.04 s, emersion 114.28 ± 0.03 s. Signal-to-noise ratios of the data, calculated from light-curve fit residuals and normalized to a 1 s cycle, are **a**, 273, **b**, 117, **c**, 108, and **d**, 28. The anomalously high points prior to immersion and post emersion in the Clay data result from the first diffraction fringe.

remained clearly resolved from Pluto–Charon, to measure the spatial offset between a standard star and C313.2. The centre of each aperture was then set by determining the centre of the comparison star and employing the offset. The sum of the signal in the aperture, minus the background, was calculated to generate light curves. The final aperture size for each dataset was selected on the basis of highest resulting signal-to-noise ratio.

Normalized light curves from each of the sites are displayed in Fig. 2. Data from the Clay telescope had the best signal-to-noise ratio (273) and the best time resolution (0.1 s). Although Gemini South is a larger telescope, the throughput was limited by an R filter and data were taken at a significantly slower cadence (0.3 s integration time, with $\sim$0.15 s deadtime). The spatial resolutions of the datasets are 2.13 km (Clay), 4.27 km (du Pont), 10.66 km (Gemini South) and 10.67 km (Cerro Armazones). These values extend from less than two to just over eight times the Fresnel scale ($\sqrt{\lambda D/2} = 1.27$ km, where wavelength λ is 720 nm and D is the distance to Charon).

Models for straight-edge diffraction by a limb, integrated over the exposure interval for each frame, were fitted separately to the immersion and emersion portions of each light curve. Free parameters of the models included background, full scale, geometric limb occultation time, and effective wavelength. As the dominant averaging effect was integration time, the occulted star was assumed to be a point source, and effects due to transfer time and smearing over a large band of wavelengths were not included. The resulting geocentric limb occultation times at each site were used to calculate Charon's radius. We have assumed that Charon is spherical and reserve asymmetric shape analysis for future work.

We find that the mean radius of Charon is 606 ± 8 km. The formal radius error from the least-squares fit to a strict circular solution is much smaller (0.04 km) because of our excellent time resolution; however, we feel that this is an underestimate given the sparse sampling of the limb and a suggestion of non-circularity from the Gemini South chord length. Further details concerning our calculation of the radius and error bar are available in Supplementary Information. The radius we find is consistent with previous measurements[5] and the lower limit established from the previous stellar occultation observation[4]. Assuming that Charon is spherical and has

Table 1 | Upper limits on atmosphere candidate gases

Gas	Molecular weight (a.m.u.)	Refractivity* (10^{-4})	Scale height† (km)	Number density upper limit‡ (10^{13} cm^{-3})	Column height upper limit‡ (cm am)
CH$_4$	16.04	4.37	90 ± 13	2.0	7.8
H$_2$O	18.02	2.50	79 ± 12	3.4	11.4
Ne	20.18	0.67	71 ± 10	11.9	36.0
N$_2$	28.01	2.95	51 ± 8	2.3	5.0
CO	28.01	3.33	51 ± 8	2.0	4.4
Ar	39.95	2.83	36 ± 5	2.0	3.1
CO$_2$	44.01	4.47	32 ± 5	1.2	1.7
Kr	83.80	4.25	17 ± 3	0.9	0.7
Xe	131.29	6.97	11 ± 2	0.4	0.2

*At standard temperature and pressure, for wavelengths ranging from 6,438 to 7,056 Å (ref. 11).
†Assuming Charon is spherical, with radius 606 ± 8 km, mass (1.60 ± 0.12) × 10^{24} g, and surface temperature 50 K.
‡Upper limits are 3σ, for an isothermal atmosphere. The number density limit applies to surface density. The upper limits on column height are written in units of centimetre amagats (cm am).

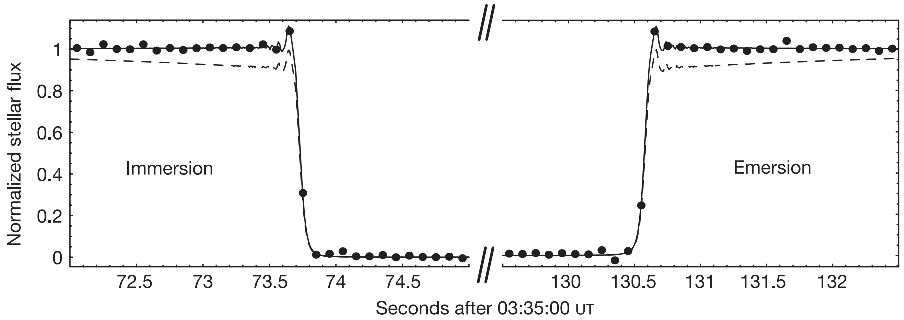

Figure 3 | Atmospheric model fits to the light-curve data. The segments of the Clay light curve shown here have been expanded such that individual data points are resolved, and the first diffraction fringe is clearly visible during immersion and emersion. A diffraction model with a tenuous atmosphere (solid line), from which our 3σ upper limit is derived, is displayed. To illustrate the effect of a substantial atmosphere, a second model is also shown (dashed line), which represents a 50-km scale height and a 10% flux drop at the surface ($b = 0.10$). This model merges with the data baseline beyond the limits of the plot. The differential bending in the dashed-line model has been enhanced significantly with respect to our upper limit ($b = 0.015$).

a mass of $(1.60 \pm 0.12) \times 10^{24}$ g (ref. 2), we find its density to be 1.72 ± 0.15 g cm^{-3}. For ice density 1.0 g cm^{-3} and rock density 3.0 g cm^{-3}, we derive a rock-mass fraction of 0.63 ± 0.05. This value suggests that Charon contains a smaller fraction of rock by mass than Pluto (0.73 ± 0.06; refs 2, 5) and Neptune's moon Triton (0.77 ± 0.01; ref. 8).

We utilized the detection of the first diffraction fringe in the Clay data to perform model fitting for a thin, isothermal atmosphere in the presence of limb diffraction[9,10]. Additional parameters for this model included atmospheric scale height and differential bending (H and b)[9], in the regime where H is much greater than the Fresnel scale. For small flux drops, the differential bending parameter b equals the drop in normalized flux at the surface radius. We selected several likely atmospheric constituents[4], listed in Table 1. The diffraction models were run over the range of scale heights appropriate for these candidates. Based on the lack of significant flux drop in the data (indicative of no significant atmosphere), we set a 3σ upper limit for differential bending of $b = 0.015$. Figure 3 shows the tenuous-atmosphere model from which this limit was derived (solid line), along with data from the Clay light curve to which it was fitted. The dashed-line model in Fig. 3 illustrates the effect of an atmosphere an order of magnitude denser than the upper limit of the fitted model. From our upper limit on b, we derive a 3σ upper limit on the refractivity for an atmosphere composed of each candidate gas[4]. Refractivities of the gases at standard temperature and pressure[11] were then used to calculate upper limits on number density and column height.

The 3σ upper limits on number density for each of the prospective atmospheric constituents are listed in Table 1. The corresponding column heights are roughly a factor of two lower than those established from the previously observed stellar occultation by Charon[4]. Such low densities are consistent with Charon's anticipated high atmospheric loss rate and lack of replenishment mechanism[12,13]. In context, the upper limits found here are orders of magnitude less than the density of N_2 near the surface of Triton ($\sim 10^{15}$ cm^{-3}; ref. 14) and at a radial distance of 1,205 km (the 3-μbar pressure level in 2002) on Pluto (2.2×10^{14} cm^{-3}; refs 14–16). More apt comparisons are the tenuous atmospheres of Io, which is primarily SO_2 and has a number density of a few times 10^{10} cm^{-3} (ref. 17), and Mercury, with a total subsolar atmospheric density of $<10^{7}$ cm^{-3} (ref. 18). Leading candidate gases of which a tenuous atmosphere on Charon may be composed are H_2O, N_2, Ar (ref. 19) and CO (ref. 20). Spectroscopic observations of Charon's surface indicate the presence of H_2O ice[21,22] mixed with a neutral absorber[23]. Other studies have suggested that volatiles could be present on the surface[24], perhaps located in shadowed regions[13]. However, the low vapour pressure of H_2O renders it an unlikely atmospheric constituent[4] and recent spectral analyses find no indication of volatile ices such as CO, CH_4 or N_2 on Charon's surface[23]. The absence of an obvious atmospheric candidate gas is consistent with the lack of a significant atmosphere in the occultation data.

The rock-mass fraction we find for Charon, in addition to those of Pluto and Triton, is higher than the maximum (~ 0.5) predicted by models of outer solar nebula condensates[8]. One explanation is a collisional origin for Pluto–Charon, during which there was a possibility for jetting of icy mantle material[6]. Charon's effective lack of atmosphere could also be explained by a volatile-removing collision[6]. The density we find for Charon is lower than the system mean, which seems consistent with an impact if either precursor object were differentiated[6]. In this case, an impactor could have collided with a differentiated proto-Pluto, leaving a disk of preferentially lower-density material that resulted in a satellite depleted in heavier elements (a situation that has a parallel in the Earth–Moon system)[6,25].

This successful observation of a stellar occultation by Charon is encouraging for establishing sizes and probing for atmospheres of large Kuiper belt objects, such as the newly discovered 2003 UB_{313}, 2005 FY_9 and 2003 EL_{61} (ref. 26). In particular, 2003 UB_{313} has approximately Charon's angular diameter and is a prime candidate for having a bound atmosphere, because methane has been detected on its surface[27] and it is larger than Pluto.

Received 2 August; accepted 21 September 2005.

1. Null, G. W. & Owen, W. M. J. Charon/Pluto mass ratio obtained with HST CCD observations in 1991 and 1993. *Astron. J.* **111,** 1368–1381 (1996).
2. Olkin, C. B., Wasserman, L. H. & Franz, O. G. The mass ratio of Charon to Pluto from Hubble Space Telescope astrometry with Fine Guidance Sensors. *Icarus* **164,** 254–259 (2003).
3. Walker, A. R. An occultation by Charon. *Mon. Not. R. Astron. Soc.* **192,** 47p–50p (1980).
4. Elliot, J. L. & Young, L. A. Limits on the radius and a possible atmosphere of Charon from its 1980 stellar occultation. *Icarus* **89,** 244–254 (1991).
5. Tholen, D. J. & Buie, M. W. in *Pluto and Charon* (eds Stern, S. A. & Tholen, D. J.) 193–219 (Univ. Arizona Press, Tucson, 1997).
6. McKinnon, W. B. On the origin of the Pluto-Charon binary. *Astrophys. J.* **344,** L41–L44 (1989).
7. McDonald, S. W. & Elliot, J. L. Pluto-Charon stellar occultation candidates: 2000–2009. *Astron. J.* **119,** 1999–2007 (2000); Erratum. **120,** 1599 (2000).
8. McKinnon, W. B., Simonelli, D. P. & Schubert, G. in *Pluto and Charon* (eds Stern, S. A. & Tholen, D. J.) 295–343 (Univ. Arizona Press, Tucson, 1997).
9. French, R. G. & Gierasch, P. J. Diffraction calculation of occultation light curves in the presence of an isothermal atmosphere. *Astron. J.* **81,** 445–451 (1976).
10. Bartholdi, P. & Owen, F. The occultation of Beta Scorpii by Jupiter and Io. II. Io. *Astron. J.* **77,** 60–65 (1972).
11. National Research Council (U.S.). *International Critical Tables of Numerical Data, Physics, Chemistry, And Technology* (eds West, C. J. & Hull, C.) (McGraw-Hill Book Co., New York, 1933).

12. Trafton, L., Stern, S. A. & Gladstone, G. R. The Pluto-Charon system: The escape of Charon's primordial atmosphere. *Icarus* **74,** 108–120 (1988).
13. Yelle, R. V. & Elliot, J. L. in *Pluto and Charon* (eds Stern, S. A. & Tholen, D. J.) 347–390 (Univ. Arizona Press, Tucson, 1997).
14. Elliot, J. L., Person, M. J. & Qu, S. Analysis of stellar occultation data. II. Inversion, with application to Pluto and Triton. *Astron. J.* **126,** 1041–1079 (2003).
15. Elliot, J. L. *et al.* The recent expansion of Pluto's atmosphere. *Nature* **424,** 165–168 (2003).
16. Pasachoff, J. M. *et al.* The structure of Pluto's atmosphere from the 2002 August 21 stellar occultation. *Astron. J.* **129,** 1718–1723 (2005).
17. Spencer, J. *et al.* Mid-infrared detection of large longitudinal asymmetries in Io's SO_2 atmosphere. *Icarus* **176,** 283–304 (2005).
18. Broadfoot, A. L., Shemansky, D. E. & Kumar, S. Mariner 10: Mercury atmosphere. *Geophys. Res. Lett.* **3,** 577–580 (1976).
19. Stern, S. A. & Trafton, L. Constraints on bulk composition, seasonal variation, and global dynamics of Pluto's atmosphere. *Icarus* **57,** 231–240 (1984).
20. Yelle, R. V. & Lunine, J. I. Evidence for a molecule heavier than methane in the atmosphere of Pluto. *Nature* **339,** 288–290 (1989).
21. Marcialis, R. L., Rieke, G. H. & Lebofsky, L. A. The surface composition of Charon: Tentative identification of water ice. *Science* **237,** 1349–1351 (1987).
22. Buie, M. W., Cruikshank, D. P., Lebofsky, L. A. & Tedesco, E. F. Water frost on Charon. *Nature* **329,** 522–523 (1987).
23. Buie, M. & Grundy, W. M. The distribution and physical state of H_2O on Charon. *Icarus* **148,** 324–339 (2000).
24. Roush, T. L. Charon: more than water ice? *Icarus* **108,** 243–254 (1994).
25. Canup, R. M. A giant impact origin of Pluto-Charon. *Science* **307,** 546–550 (2005).
26. Brown, M. E., Trujillo, C. A. & Rabinowitz, D. L. 2003 EL_61, 2003 UB_313, and 2005 FY_9. *IAU Circ.* **8577** (2005).
27. Trujillo, C. A., Barkume, K. M., Brown, M. E., Schaller, E. L. & Rabinowitz, D. L. Near infrared spectra from Mauna Kea of the new brightest Kuiper Belt Object. *Bull. Am. Astron. Soc.* **37,** 52.06 (2005).
28. USNO. *The Astronomical Almanac for the Year 2005* (US Govt Printing Office, Washington DC, 2003).

Supplementary Information is linked to the online version of the paper at www.nature.com/nature.

Acknowledgements B.A.B., J.W.G. and T.T. are Guest Observers at Instituto de Astronomía, Universidad Católica del Norte, Antofagasta, Chile. We thank N. Vogt and M. Murphy of Universidad Católica del Norte for their expertise, assistance, and the use of their telescope at Cerro Armazones; G. Gutiérrez and F. Sánchez, telescope operators at Las Campanas; R. Carrasco, K. Volk (observers), and E. Wendroth (telescope operator) at Gemini South; M. Ottoboni and R. Campos at Pico Dos Dias; and C. Czelusniak, assistant observer from Universidade Estadual de Ponta Grossa. Full credits for Gemini Observatory are available at http://www.us-gemini.noao.edu/sciops/data/dataAcknowIndex.html. Support for this work was provided by NASA Planetary Astronomy. Additional support was provided by the Belgian Federal Office for Scientific, Technical and Cultural Affairs and the Flemish Ministry for Foreign Policy, European Affairs, Science and Technology.

Author Information Reprints and permissions information is available at npg.nature.com/reprintsandpermissions. The authors declare no competing financial interests. Correspondence and requests for materials should be addressed to A.A.S.G. (gulbis@mit.edu).